Bioconjugate Chemistry

Article

Cite This: *Bioconjugate Chem.* 2018, 29, 928−938

pubs.acs.org/bc

# Enhanced Cellular Ablation by Attenuating Hypoxia Status and Reprogramming Tumor-Associated Macrophages via NIR Light-Responsive Upconversion Nanocrystals

Xiangzhao Ai,[†] Ming Hu,[†] Zhimin Wang,[†] Linna Lyu,[†] Wenmin Zhang,[†,‡] Juan Li,[‡] Huanghao Yang,[‡] Jun Lin,[§] and Bengang Xing*[,†,‡]

[†]Division of Chemistry and Biological Chemistry, School of Physical & Mathematical Sciences, Nanyang Technological University, Singapore, 637371, Singapore

[‡]College of Chemistry, Fuzhou University, Fuzhou, Fujian 350116, China

[§]State Key Laboratory of Rare Earth Resource Utilization, Changchun Institute of Applied Chemistry, Chinese Academy of Sciences, Changchun, 130022, China

*S* *Supporting Information*

**ABSTRACT:** Near-infrared (NIR) light-mediated photodynamic therapy (PDT), especially based on lanthanide-doped upconversion nanocrystals (UCNs), have been extensively investigated as a promising strategy for effective cellular ablation owing to their unique optical properties to convert NIR light excitation into multiple short-wavelength emissions. Despite the deep tissue penetration of NIR light in living systems, the therapeutic efficiency is greatly restricted by insufficient oxygen supply in hypoxic tumor microenvironment. Moreover, the coexistent tumor-associated macrophages (TAMs) play critical roles in tumor recurrence during the post-PDT period. Herein, we developed a unique photosensitizer-loaded UCNs nanoconjugate (PUN) by integrating manganese dioxide ($MnO_2$) nanosheets and hyaluronic acid (HA) biopolymer to improve NIR light-mediated PDT efficacy through attenuating hypoxia status and synergistically reprogramming TAMs populations. After the reaction with overproduced $H_2O_2$ in acidic tumor microenvironment, the $MnO_2$ nanosheets were degraded for the production of massive oxygen to greatly enhance the oxygen-dependent PDT efficiency upon 808 nm NIR light irradiation. More importantly, the bioinspired polymer HA could effectively reprogram the polarization of pro-tumor M2-type TAMs to anti-tumor M1-type macrophages to prevent tumor relapse after PDT treatment. Such promising results provided the great opportunities to achieve enhanced cellular ablation upon NIR light-mediated PDT treatment by attenuating hypoxic tumor microenvironment, and thus facilitated the rational design of new generations of nanoplatforms toward immunotherapy to inhibit tumor recurrence during post-PDT period.

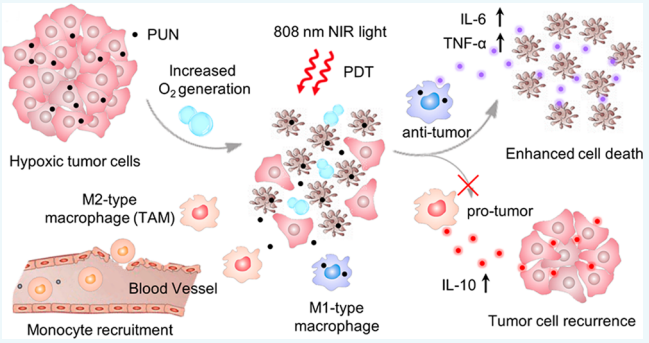


## INTRODUCTION

Currently, cancer is a leading cause of human morbidity and mortality worldwide.[1] Despite traditional therapeutic strategies (such as surgery, chemotherapy, and radiotherapy) presenting benefits in improving survival rates, great challenges still remain in the course of anticancer treatment including limited efficiency, adverse effects in normal tissues, and higher risk of tumor recurrence.[2−5] Therefore, alternative therapeutic modalities are still in high demand to benefit treatment options against malignant tumors for patients. Among various treatment approaches in recent decades, photodynamic therapy (PDT), which relies on tissue oxygen and photosensitizer (PS) agents to generate reactive oxygen species (ROS) (e.g., single oxygen ($^1O_2$), etc.) under a beam of light irradiation, has been recently considered as one of the promising therapeutic modalities for effective cancer treatment due to its specific advantages including intrinsically noninvasive safety and high spatiotemporal selectivity upon light illumination.[6−8] However, the activation wavelengths of most clinically used PS molecules usually rely on short-wavelength light (e.g., ultraviolet (UV) and visible light), which have limited tissue penetration depth and potential photodamage owing to the inherent absorption of some endogenous light chromophores including hemoglobin, flavins, and melanin.[9,10] Thus, one inspiring approach with long-wavelength near-infrared (NIR) light (700−1000 nm) irradiation, which displays deep-tissue penetration, minimized photodamage, and low autofluorescence in living systems, has been proposed as a promising method in phototheranos-

**Special Issue:** Biomimetic Materials

**Received:** January 25, 2018
**Revised:** February 20, 2018
**Published:** February 21, 2018





DOI: 10.1021/acs.bioconjchem.8b00068
*Bioconjugate Chem.* 2018, 29, 928−938

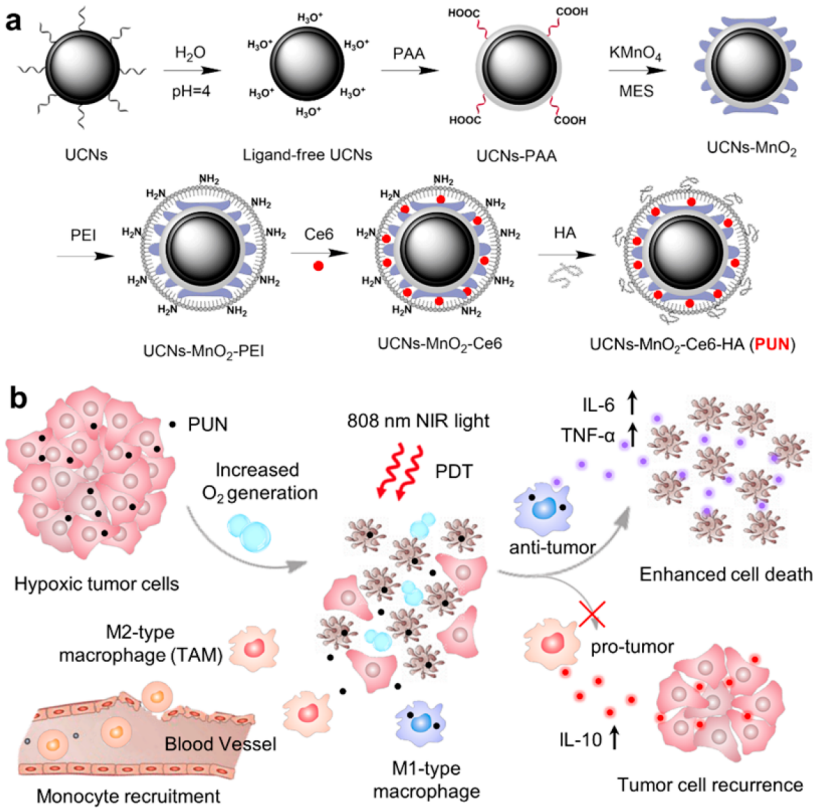


**Figure 1.** Illustration of NIR light-mediated PDT strategy for the enhanced cellular ablation in tumor microenvironment. (a) Design and synthesis of PUN (UCNs-$MnO_2$-Ce6-HA). (b) Scheme of improved therapy by attenuating hypoxia status and reprogramming tumor-associated macrophages (TAMs) from M2 to M1 phenotype to inhibit the recurrence of tumor cells toward immunotherapy during the post-PDT period.

tics.[11−14] Despite a few NIR-light-responsive PS molecules have been utilized for PDT studies in recent years, several inevitable drawbacks, such as troublesome synthetic procedures and limited $^1O_2$ generation capabilities, heavily restrict their further therapeutic applications.[15,16] Therefore, the development of innovative strategies that allow deep-tissue penetration with effective PDT as well as negligible normal tissue damage is highly desirable.

Recently, lanthanide-doped upconversion nanocrystals (UCNs) have emerged and gained significant interest in material science due to their unique optical properties to convert NIR light into broad UV/visible emission,[17−21] which provide a powerful tool to activate various PS upon NIR light irradiation to overcome the tissue penetration and safety issues of current PDT approaches.[22−26] Despite initial successes, the oxygen-dependent nature of PDT greatly restricts its effectiveness in the hypoxic tumor microenvironment due to insufficient oxygen supply in tumor vascular systems.[27−30] So far, several strategies have been developed to alleviate tumor hypoxia such as inhibiting oxygen consumption in tumor cells by mitochondrial respiration inhibitors or increasing oxygen supply to the tumor regions with hyperbaric oxygen treatment and vasoactive drugs.[31] Nonetheless, the clinical utilities of these methods are limited by multiple constraints including potential safety concerns, low oxygen-carrying capacities, and inadequate delivery efficiencies to the hypoxia regions.[32,33] More importantly, the principal coexistent host macrophage cell populations in solid tumors, known as tumor-associated macrophages (TAMs), play complex but pivotal roles in the outcome of PDT in tumor microenvironment such as cancer recurrence, invasion, angiogenesis, and metastases.[34,35] Normally, macrophages are characterized as two distinct populations, classically activated pro-inflammatory (M1) phenotype (attacking invaders) and alternatively activated anti-inflammatory (M2) phenotype (healing damages).[36] The polarization of macrophage is a highly dynamic process and the phenotype of M1- or M2-polarized macrophages can be reversed depending on the different physiological and pathological environments. During post-PDT period, the residual tumor cells will release chemo-attractants to mobilize the steady recruitment of monocytes from the peripheral blood, and these monocytes will quickly differentiate into TAMs to support tumor progression by adopting an M2 phenotype to produce pro-tumor cytokines (e.g., interleukin 10 (IL-10)), and thereby to promote tissue repair and tumor recurrence including angiogenesis, matrix remodeling, and immunosuppression.[37,38] In contrast, the macrophages with M1-type polarization are extremely deficient, which exhibit classic anti-tumor activity to inhibit the cell growth by secreting multiple cytotoxic cytokines such as tumor necrosis factor alpha (TNF-$\alpha$) and interleukin 6 (IL-6).[39,40] Therefore, the development of effective strategy to improve the PDT efficiency by increasing the oxygen amounts in hypoxia environment as well as reprograming the TAMs phenotype for tumor recurrence inhibition during post-PDT period, is in high demand, and relevant investigations are still limited so far.

In this work, as proof-of-concept, we presented a unique PS-loaded UCNs nanoconjugate (PUN) to enhance the efficacy of NIR light-mediated cellular ablation through attenuating hypoxia status and synergistically reprogramming TAMs populations (Figure 1). In order to increase the oxygen supply in hypoxia conditions, manganese dioxide ($MnO_2$) nanosheets


DOI: 10.1021/acs.bioconjchem.8b00068
Bioconjugate Chem. 2018, 29, 928−938

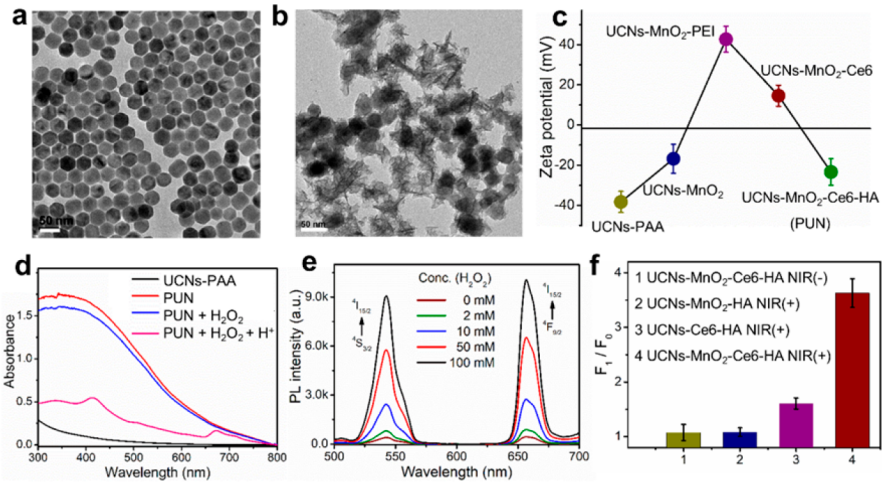


**Figure 2.** Characterization of PUN (UCNs-$MnO_2$-Ce6-HA) in buffers. TEM images of (a) UCNs and (b) PUN. Scale bar: 50 nm. (c) Zeta potential of various nanostructures during the synthesis process of PUN. (d) UV−vis spectra of PUN (1 mg/mL) before and after reaction with $H_2O_2$ (10 mM) in neutral (pH = 7.4) and acid ($H^+$) solutions (pH = 5.5). (e) UCL spectra of PUN in the presence of different concentration of $H_2O_2$ in acid buffers. (f) $^1O_2$ production of various UCNs-based nanostructures in acid and hypoxic environment with $H_2O_2$ upon 808 nm NIR light irradiation.

were modified on the surface of PUN, which could be degraded to generate plenty of oxygen upon the reaction with overproduced $H_2O_2$ in the acidic tumor microenvironment.[41,42] Under 808 nm NIR light irradiation, the upconverted emission at 655 nm could effectively activate the loaded PS molecules, chlorin-e6 (Ce6), to produce more cytotoxic $^1O_2$ based on the improved oxygen level for enhanced PDT treatment. More significantly, inspired by the attractive properties of hyaluronic acid (HA), a natural glycosaminoglycan which could regulate the activation states between pro-tumor M2-type and anti-tumor M1-type macrophage,[43−45] we modified HA as a functional biopolymer on the outer layer of PUN to achieve the immunomodulation of TAM polarization from M2 to M1 phenotype, which exhibited strong inhibition of tumor recurrence after PDT treatment. Such promising studies may hold the great potential to dramatically enhance NIR light-mediated PDT efficiency in a hypoxic microenvironment as well as to prevent the relapse of malignancies toward immunotherapy during post-PDT period.

## RESULT AND DISCUSSION

Figure 1 illustrates the design of NIR light-mediated PUN for enhanced therapeutics in the hypoxic tumor microenvironment as well as immunomodulation of the TAMs phenotype to inhibit cancer recurrence. Generally, the core−shell UCNs were prepared according to a previously established thermal decomposition method in our group. In order to minimize the undesired overheating effect typically associated with conventional 980 nm laser irradiation, $Nd^{3+}$-sensitized lanthanide-doped nanoparticles were constructed to improve pumping efficiency at 808 nm (Figure S1, Supporting Information). Transmission electron microscopy (TEM) revealed that the UCNs had uniform hexagonal morphology with a narrow size distribution of 38 ± 3 nm (Figure 2a and Figure S1). In order to increase the solubility of UCNs in water, the surface-anchored hydrophobic ligands (oleic acid) were removed in acid solution and the ligand-free nanoparticles were further modified by poly(acrylic acid) (PAA) to prepare hydrophilic nanostructures (UCNs-PAA). Moreover, the formation of amorphous $MnO_2$ nanosheets enwrapped on the membrane of UCNs-PAA (UCNs-$MnO_2$) was achieved by the redox reaction between potassium permanganate ($KMnO_4$) and 2-(N-morpholino)ethanesulfonic acid (MES) to generate Mn−O bonding via coordination interaction,[41,46] which was confirmed by transmission electron microscopy (TEM), UV−vis spectroscopy, and Fourier transform infrared (FTIR) spectroscopy (Figures S1, S2, and S3). The synthesized UCNs-$MnO_2$ was further coated with amino-contained polyethylenimine (PEI) to facilitate subsequent surface modification.[47]

To ensure the therapeutic efficiency, an effective PS molecule (Ce6) was anchored on the surface of UCNs-$MnO_2$-PEI by amide condensation (UCNs-$MnO_2$-Ce6) based on the favorable overlap between specific absorption spectrum of Ce6 and the upconverted luminescences (UCL) signal of UCNs at 655 nm upon 808 nm laser excitation (Figure S4).[48] Furthermore, to achieve the immunomodulation of TAMs polarization, a natural biopolymer HA was finally regarded as the outer layer of PUN (Figure 2b and Figure S1). The successful localization of Ce6 and HA on the UCNs nanoplatform were demonstrated by UV−vis spectroscopy and FTIR characterization, respectively (Figures S3 and S5). The optimal amount of Ce6 was determined to be 5.2%, and there was 21.5 $\mu$M/mg HA detected on the PUN (Figures S6 and S7). In addition, the zeta potential of these UCNs-based nanoparticles were monitored from UCNs-PAA (−38.3 mV), UCNs-$MnO_2$ (−16.8 mV), UCNs-$MnO_2$-PEI (+42.7 mV) to UCNs-$MnO_2$-Ce6 (+14.6 mV) and UCNs-$MnO_2$-Ce6-HA (−23.4 mV), respectively (Figure 2c), demonstrating the successful modification of different polymers on the surface of UCNs. These results were also confirmed by the increased hydrodynamic diameter of these nanoparticles in aqueous solution by dynamic light scattering (DLS) (Figure S8). Moreover, due to the great overlap between the broad absorption spectrum of $MnO_2$ nanosheets and the specific emission spectra of UCNs and Ce6, respectively, the UCL signals of UCNs and fluorescence of Ce6 were significantly quenched (Figures S9 and S10). The prepared PUN dispersed well in deionized water and presented almost unchanged absorption spectra after storage at room temperature for 1 week, indicating the great solubility and stability of PUN in buffers (Figure S11).



DOI: 10.1021/acs.bioconjchem.8b00068
Bioconjugate Chem. 2018, 29, 928−938

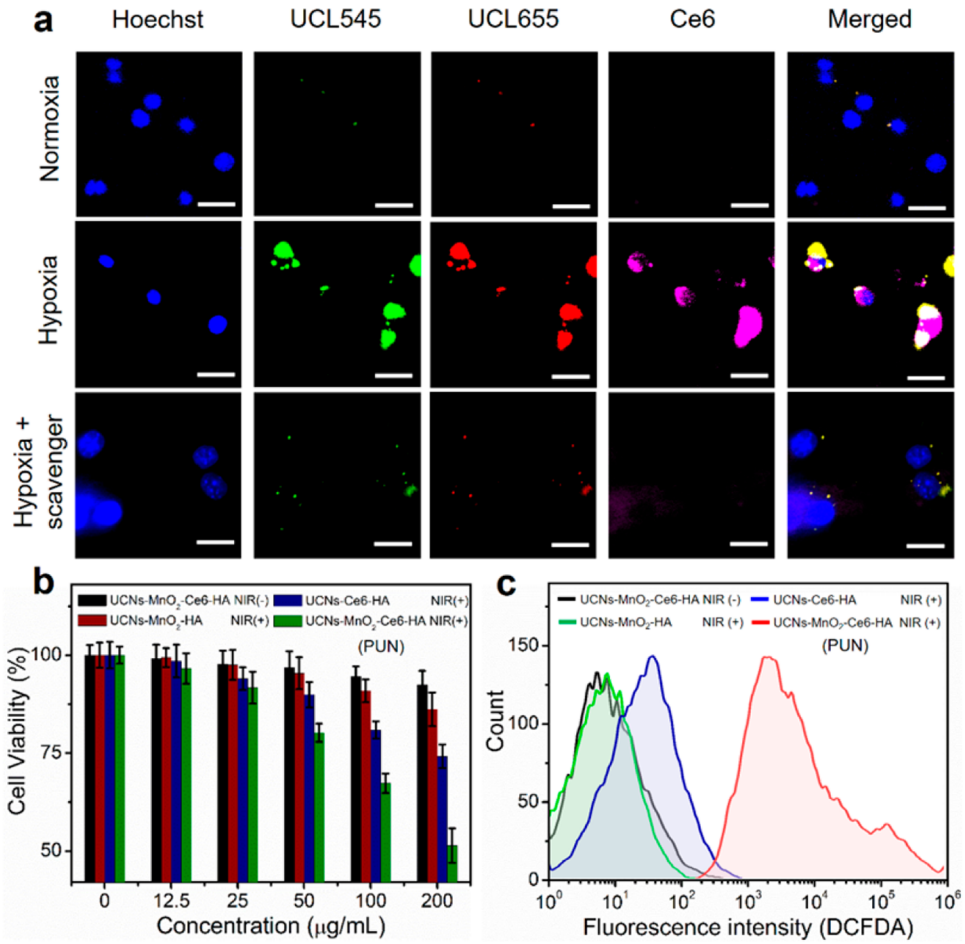


**Figure 3.** Enhanced PDT efficiency of PUN (UCNs-$MnO_2$-Ce6-HA) in hypoxic tumor cells. (a) Confocal imaging of PUN in cells with different conditions of normoxia, hypoxia, and hypoxia with $H_2O_2$ scavenger, respectively. Blue: Hoechst ($E_x$: 350/50 nm, $E_m$: 460/50 nm); green: UCL at 545 nm ($E_x$: 980 nm, $E_m$: 530/50 nm); red: UCL at 655 nm ($E_x$: 980 nm, $E_m$: 610/75 nm); violet: Ce6 ($E_x$: 545/25 nm, $E_m$: 610/75 nm). Scale bar: 20 $\mu$m. (b) Cell viability of tumor cells with different concentrations of PUN upon 808 nm NIR light irradiation (0.4 W/cm$^2$) for 1 h. (c) FCM analysis of elevated intracellular ROS level by a ROS indicator (DCFDA) ($E_x$: 488 nm, $E_m$: 510/21 nm).

We subsequently evaluated the feasibility of whether the $MnO_2$ nanosheets could catalyze the generation of oxygen in the presence of $H_2O_2$ in acid buffer solutions. As shown in Figure 2d, the strong absorption spectra of PUN (UCNs-$MnO_2$-Ce6-HA) presented an obvious decrease at acid solution (pH = 5.5) along with the appearance of specific peak of Ce6 (~655 nm) upon incubation with $H_2O_2$ (10 mM) for 30 min, while it remained almost unchanged in neutral solutions (pH = 7.4) at the same conditions. Moreover, plenty of gas bubbles were produced in the solution of PUN in the presence of $H_2O_2$ followed by the color change from dark to light brown in acidic buffers. These results demonstrated that the $MnO_2$ was decomposed by the reaction with $H_2O_2$ to produce abundant gases in acid solution. According to the established chemical eq 1[41,42,49]

$$MnO_2 + H_2O_2 + 2H^+ \rightarrow Mn^{2+} + O_2 \uparrow + 2H_2O \quad (1)$$

the decomposition reaction of $MnO_2$ demands the consumption of $H_2O_2$ and $H^+$ ions, simultaneously generating $O_2$ and $Mn^{2+}$ ions. Interestingly, it is well-known that the tumor microenvironment is characterized by overproduction of $H_2O_2$ and lower pH value than surrounding normal tissues. On one hand, tumor cells are metabolically hyperactive leading to the massive consumption of $O_2$ and generation of excessive ROS levels including $H_2O_2$ in cancer stroma. On the other hand, solid tumors had a unique metabolic profile to produce large quantities of lactic acid to reduce the pH values based on the enhanced glycolysis during tumorigenesis. Thus, the degradation of $MnO_2$ exhibited specific selectivity to the tumor regions rather than healthy tissues based on the overproduced $H_2O_2$ levels and acidic conditions in hypoxic microenvironment. Moreover, after the decomposition of $MnO_2$ nanosheets, the quenched UCL signals of UCNs and fluorescence emission of Ce6 were gradually recovered with the increasing concentrations of $H_2O_2$ in acid buffers (Figure 2e and Figure S12), suggesting that the PUN could be regarded as an effective biosensor to monitor the existent $H_2O_2$ in buffers by utilizing the emission of UCNs and Ce6, respectively.

To further verify the capability of PUN to produce more $^1O_2$ based on the enhanced oxygen level, we also evaluated $^1O_2$ generation at hypoxic environment through the standard singlet oxygen sensor green (SOSG), which could specifically react with $^1O_2$ to cause fluorescence increase at 530 nm.[50] As shown in Figure 2f, very little $^1O_2$ generation was determined for PUN without NIR light excitation (group 1) and for UCNs-$MnO_2$-HA with light irradiation (group 2), indicating that the NIR light or the particle itself had negligible effects on the $^1O_2$ formation. However, the remarkable increment (~3.6-fold increase) of green fluorescence intensity for PUN (group 4)


DOI: 10.1021/acs.bioconjchem.8b00068
Bioconjugate Chem. 2018, 29, 928−938

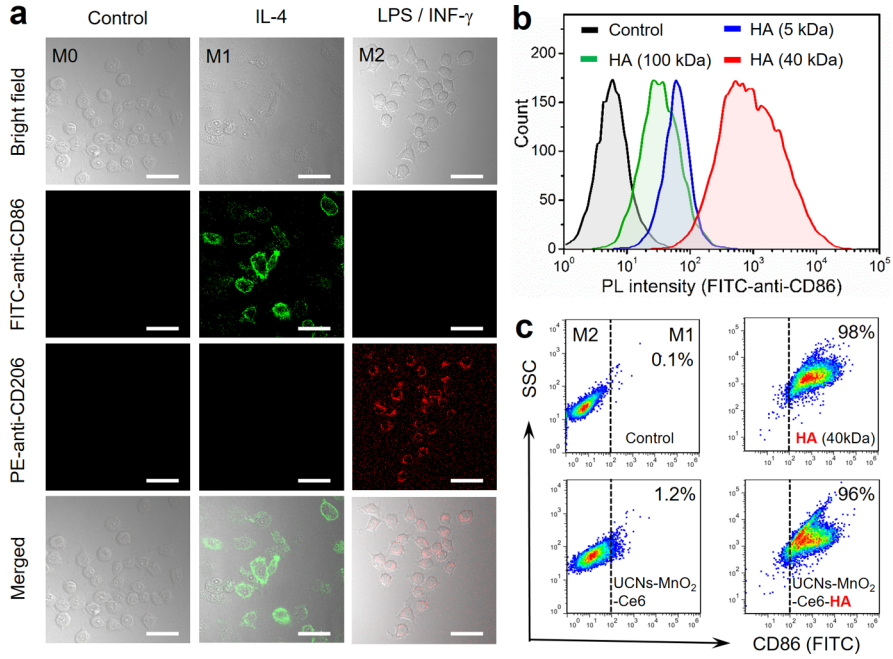


**Figure 4.** Reprograming of the macrophages from M2 to M1 phenotype by PUN (UCNs-$MnO_2$-Ce6-HA) in RAW264.7 cells. (a) Confocal imaging of macrophages with M0 (monocyte), M1, and M2 phenotype upon IL-4 and LPS/IFN-$\gamma$ stimulation, and immunostaining with FITC-anti-CD86 or PE-anti-CD206, respectively. Green: FITC ($E_x$: 488 nm, $E_m$: 510/21 nm); red: PE ($E_x$: 543 nm, $E_m$: 580/50 nm). Scale bar: 50 $\mu$m. (b,c) FCM analysis of the reprogramed M1-type macrophages from M2-type (TAMs) after incubation with HA biopolymer (1 $\mu$M) at different molecular weight (b) and PUN nanoplatform (c). FITC-anti-CD86: $E_x$: 488 nm, $E_m$: 530/50 nm.

was higher than that for UCNs-Ce6-HA (~1.6-fold increase in group 3), indicating that the greatly elevated $^1O_2$ production was achieved owing to the enhanced oxygen supply in hypoxic conditions upon NIR light treatment. All of these results strongly demonstrated that PUN could effectively increase oxygen amounts by decomposing $MnO_2$ nanosheets with $H_2O_2$ in acidic condition, which had great potential to promote more cytotoxic $^1O_2$ generation for the enhanced PDT efficacy in hypoxic tumor microenvironment.

Encouraged by these promising results, we further explored the applications of PUN for enhanced tumor cell ablation. In order to mimic the endogenous $H_2O_2$ generation in hypoxic microenvironment, as a model, the murine melanoma cell line (B16F10) was incubated with PUN (100 $\mu$g/mL) and cultured for 24 h in a pouch anaerobic system.[51] As shown in Figure 3a, in normoxic condition, no obvious UCL signals and Ce6 fluorescence were noticed owing to the quenching effects by $MnO_2$ nanosheets. However, in the hypoxic conditions, the significant fluorescent increment of UCL signals at 545 nm (red), 655 nm (green), and emissions of Ce6 at 675 nm (violet) were observed clearly, which was confirmed by the control experiment upon the pretreatment of $H_2O_2$ scavenger (sodium pyruvate, 10 mM). These results indicated that the effective cellular internalization of PUN and the presence of endogenous $H_2O_2$ in hypoxic tumor cells to induce the decomposition of $MnO_2$ and production of oxygen for further PDT treatment.

Inspired by these imaging results, we further evaluated the therapeutic effects of PUN in hypoxia microenvironment through a standard *in vitro* toxicology assay (TOX8) upon NIR light irradiation.[52] As shown in Figure 3b, there was high cell viability (>90%) in the PUN-incubated B16F10 cells without light exposure, suggesting minimum toxicity caused by the particle itself. However, upon 808 nm laser irradiation (0.4 W/cm$^2$) for 1 h, a higher cytotoxicity (~51% cell viability) was observed with PUN (200 $\mu$g/mL) incubation than that of cells in control groups treated with the UCNs-$MnO_2$-HA (~86% cell viability) or UCNs-Ce6-HA (~74% cell viability) in hypoxic conditions. The enhanced cytotoxicity could be attributed to the elevated intracellular ROS level, which was confirmed by a standard fluorescent ROS indicator (2′,7′-dichlorofluorescin diacetate, DCFDA) in tumor cells.[53] As shown in Figure 3c and Figure S13, both of the quantitative flow cytometry (FCM) analysis and confocal imaging indicated that the cells incubated with PUN under NIR light treatment exhibited an increased fluorescence intensity than that of cells in control groups treated with the UCNs-Ce6-HA or UCNs-$MnO_2$-HA, respectively. These results successfully demonstrated that PUN presented a remarkable anti-tumor effect based on the enhanced PDT treatment upon NIR light irradiation in hypoxic tumor microenvironment.

Considering that the coexistent TAMs play critical roles in the recurrence of tumor cells during post-PDT period, ongoing explorations were performed to further improve therapeutic outcomes by reprograming the TAMs activities from pro-tumor M2 to anti-tumor M1 phenotype based on the anchored HA biopolymer on PUN surface. Normally, the models of classically (M1-like) and alternatively (M2-like) activated macrophages were established by stimulating initial murine monocyte macrophage RAW 264.7 cell line (M0-like) with interleukin 4 (IL-4) and lipopolysaccharide (LPS)/interferon-$\gamma$ (IFN-$\gamma$), respectively.[54−56] The successful polarization of monocyte macrophages to M1 or M2 phenotypes were determined by the upregulated expression of mannose receptors (CD86 marker for M1 and CD206 marker for M2), which could be specifically stained by FITC- and PE-labeled antibodies respectively for confocal imaging and FCM analysis (Figure 4a and Figure S14). More importantly,


DOI: 10.1021/acs.bioconjchem.8b00068
*Bioconjugate Chem.* 2018, 29, 928−938

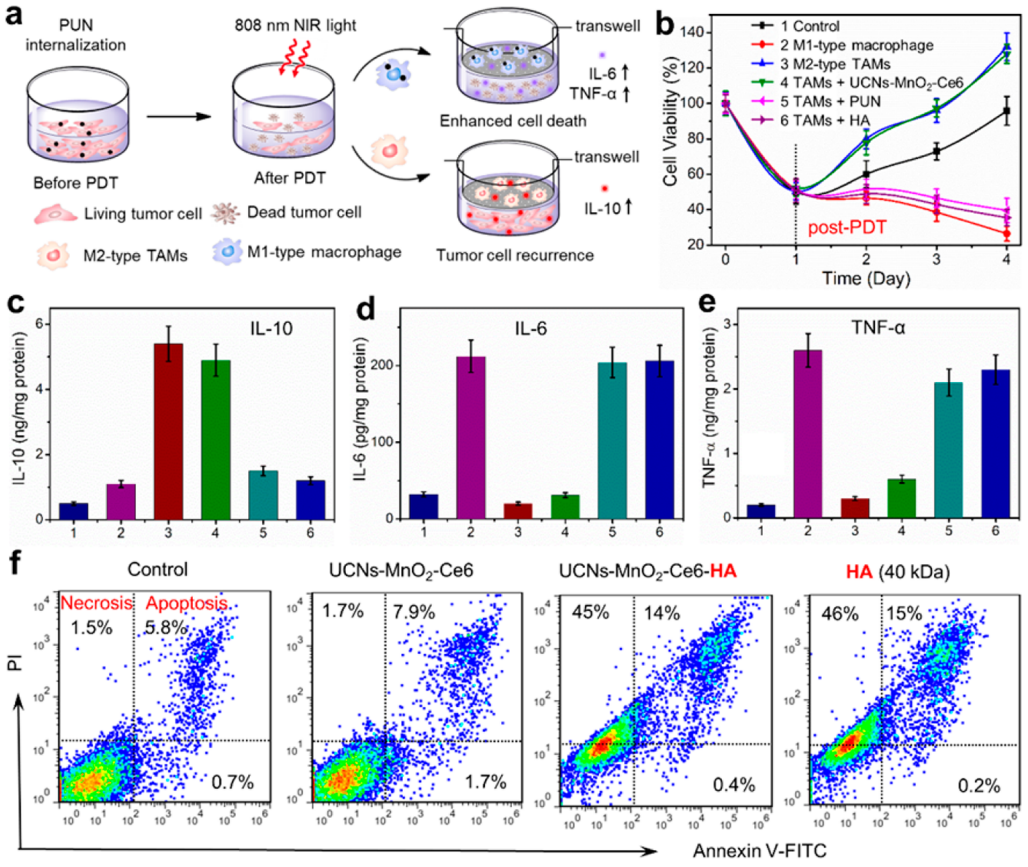


**Figure 5.** Inhibition of tumor cells recurrence by PUN (UCNs-$MnO_2$-Ce6-HA) after PDT treatment. (a) Scheme of enhanced cells ablation after incubation with reprogrammed M2-type TAMs upon PUN stimulation. (b) Cell viability of tumor cells during the post-PDT period cocultured with (1) no cells as control; (2) M1-type macrophages; (3) M2-type TAMs; (4–6) TAMs incubated with UCNs-$MnO_2$–Ce6 (4); PUN (5) and HA (6), respectively. (c–e) Quantitative cytokine analysis of pro-tumor IL-10 (c), anti-tumor IL-6 (d) and TNF-$\alpha$ (e) in different groups. (f) FCM analysis of tumor cell death process with standard annexin V-FITC/propidium iodide (PI) assay kit.

numerous studies have demonstrated that HA, a ubiquitously glycosaminoglycan of the extracellular matrix, may function as an inflammatory mediator to regulate the phenotype of macrophages based on different molecular weights.[44,45,57] In order to reprogram the macrophages from M2 to M1 phenotype, we cultured M2-type TAMs in the presence of HA biopolymer (1 $\mu$M) with different molecular weights, and detected the reversed M1-like macrophages by FCM after staining with FITC-anti-CD86. As shown in Figure 4b, the enhanced FITC fluorescence intensity in M2-like macrophage cells upon 40 kDa HA stimulation is more than that of cells incubated with HA at lower (5 kDa) and higher (100 kDa) molecular weight, indicating that M1-like macrophages were achieved upon the treatment with intermediate HA biopolymer, which may activate the innate immune response via a TLR2-MyD88-IRAK1-TRAF6-PKC$\zeta$-NK-$\kappa$B-dependent pathway as reported previously.[43,58] In line with these results, we further evaluated the efficiency of phenotype regulation from M2 to M1 macrophage upon HA-modified PUN treatment. As shown in Figure 4c, little fluorescence intensity change was detected before (0.1%) and after (1.2%) addition of UCNs-$MnO_2$-Ce6, suggesting that the particle itself indicated negligible effect for the macrophage phenotype. Upon the incubation with PUN, significant increment of FITC-anti-CD86 fluorescence signals (96%) was determined by FCM analysis, which presented a similar immunomodulation effect of macrophages under HA biopolymer stimulation (98%), demonstrating that the HA-modified PUN could act as a mediator to effectively reprogram M2-like TAMs to M1-like macrophages.

Furthermore, we also investigated the possibility whether such PUN could inhibit the recurrence of tumor cells during the post-PDT period. In order to establish the tumor cell relapse model, the B16F10 cells were first incubated with PUN (200 $\mu$g/mL) as previously for PDT treatment at hypoxia microenvironment upon 808 nm NIR light irradiation, and then the residual tumor cells were cultured for several days to promote the cell growth (Figure 5a). To understand the influence of tumor cell proliferation in the presence of macrophages at different phenotypes, we cocultured relapsed tumor cells with activated RAW264.7 cells at different conditions on the upper chamber of a permeable transwell insert. After several days' incubation, the tumor cell viabilities were determined by a standard *in vitro* toxicology assay (TOX8). As shown in Figure 5b, compared with day 1, the tumor cells at day 4 without RAW264.7 cells treatment exhibited obvious enhancement of cell viabilities (~1.9-fold increase), indicating tumor cell recurrence after PDT treatment (group 1). Interestingly, when the cells were incubated with M2-like TAMs, the cell viabilities presented higher increment (~2.6-fold increase) in group 2, suggesting the pro-tumor properties of TAMs. However, once the tumor cells were cocultured with M1-like macrophages, the remarkably decreased cell viability (~26%) was observed in group 3, indicating the anti-tumor efficiency of M1-type macrophages.



DOI: 10.1021/acs.bioconjchem.8b00068
*Bioconjugate Chem.* 2018, 29, 928–938

These results suggested that the macrophages of different phenotypes exhibited completely different effects on the growth of tumor cells. More importantly, considering that HA-modified PUN could effectively reprogram the macrophage phenotype, we further cocultured the tumor cells at post-PDT period with M2-like TAMs in transwell supports toward PUN stimulation. As shown in Figure 5b, at day 4, remarkable inhibition of tumor growth was determined by much lower cell viabilities (~39% and ~35%) after incubation with TAMs treated by PUN (group 5) or HA biopolymer (group 6), respectively, while tumor cell relapse was still observed after incubation with TAMs upon UCNs-$MnO_2$-Ce6 treatment (group 4). These results strongly demonstrated that HA-modified PUN could effectively inhibit tumor recurrence after PDT treatment based on the reprogramming of TAM activities from M2 to M1 polarization.

In order to further explore the underlying reasons for tumor cell death and relapse cocultured with macrophages on different phenotypes, we investigated the excreted cytokines by RAW264.7 cells at various activation states. It has been reported that the M2-type TAMs produce pro-tumor and cytoprotective cytokines (e.g., IL-10) to promote tissues repair, while M1-type macrophages secrete anti-tumor cytokines (e.g., IL-6 and TNF-$\alpha$) to inhibit the tumor growth. As shown in Figure 5c–e, few cytokines were detected in the medium of tumor cells without RAW264.7 cells treatment (group 1), while a high level of IL-10 was examined when the tumor recurrence occurred after incubation with M2-type TAMs (group 3), clearly suggesting that IL-10 might promote the relapse of tumor cells. Moreover, unregulated expressions of IL-6 and TNF-$\alpha$ were observed when the cell growth was inhibited upon M1-like macrophages treatment (group 2), indicating that these cytokines might prevent the recurrence of tumor cells. To further confirm our hypothesis, we incubated the tumor cells with these three cytokines respectively and detected their cell viabilities. As expected, the cells viability presented a 2.5-fold increase upon IL-10 stimulation, and 21% and 35% decrease under IL-6 and TNF-$\alpha$ treatment, respectively (Figure S15), indicating that the polarized RAW264.7 cells in different phenotypes could promote or inhibit the cell recurrence by excreting specific cytokines in the tumor microenvironment. Based on these results, we further explored the potential mechanisms for the enhanced tumor cell death cocultured with reprogrammed macrophages toward PUN stimulation. As shown in Figure 5d,e, the M2-type TAMs upon UCNs-$MnO_2$-Ce6 treatment presented low level expression of cytotoxic IL-6 and TNF-$\alpha$ (group 4). However, when the macrophages were incubated with PUN (group 5) or HA biopolymer (group 6), obvious increment of these cytokines was determined, suggesting that HA-modified PUN could regulate the anti-tumor cytokines secretion by reprogramming the TAMs phenotype to inhibit the tumor cell recurrence. Furthermore, by using FCM analysis with standard annexin V-FITC/propidium iodide (PI) assay kit, we also demonstrated that both apoptosis and necrosis occurred in the process of tumor cells death cocultured with TAMs upon HA-modified PUN treatment (Figure 5f).[59] All of these results strongly demonstrated that the PUN not only improved the PDT effect in hypoxic tumor microenvironment, but also reprogrammed the M2-like TAMs to M1-like phenotype to further prevent the tumor recurrence during the post-PDT period.

## CONCLUSIONS

In summary, we proposed a novel nanoplatform (PUN) by integrating $MnO_2$ nanosheets and HA biopolymer to improve NIR light-mediated PDT efficacy in hypoxia tumor microenvironment and to inhibit tumor recurrence by reprogramming TAMs populations during the post-PDT period. Upon reaction with overproduced $H_2O_2$ in the acidic tumor microenvironment, the $MnO_2$ nanosheets were degraded for the production of massive amounts of oxygen to greatly increase the oxygen-dependent PDT efficiency upon 808 nm NIR light irradiation. More importantly, the bioinspired HA polymer could effectively reprogram the polarization from pro-tumor M2-type TAMs to anti-tumor M1-type macrophages to inhibit tumor relapse after PDT treatment. Such promising studies not only provide an attractive opportunity to greatly enhance the NIR light-mediated cellular ablation efficiency in hypoxic tumor microenvironment, but also significantly facilitate the rational design of new generations of nanoplatforms toward immunotherapeutic approaches to regulate the macrophages phenotypes, which holds excellent potential to avoid the recurrence of various malignant tumors in the future.

## EXPERIMENTAL PROCEDURES

**Materials and Methods.** $Y(CH_3CO_2)_3$, $Yb(CH_3CO_2)_3$, $Er(CH_3CO_2)_3$, $Nd(CH_3CO_2)_3$, oleic acid, 1-octadecene, $NH_4F$, NaOH, poly(acrylic acid) (PAA, Mw 1800), 2-(*N*-morpholino)ethanesulfonic acid (MES), polyethylenimine (PEI, Mw 25000, branched), 1-ethyl-3-(3-(dimethylamino)-propyl) carbodiimide hydrochloride (EDC·HCl), *N*-hydroxysuccinimide (NHS), singlet oxygen sensor green (SOSG), in vitro toxicology assay kit (TOX8, resazurin based), Hoechst 33342 (bisBenzimideH 33342trihydrochloride), 2′,7′-dichlorofluorescin diacetate (DCFDA), Corning transwell inserts (12 well, 0.4 $\mu$m pore), and Annexin V-FITC apoptosis detection kit were purchased from Sigma-Aldrich. Dulbecco's Modified Eagle Medium (DMEM), fetal bovine serum (FBS), penicillin-streptomycin, and trypsin-EDTA were obtained from Invitrogen (Carlsbad, CA, USA). The GasPak pouch anaerobic system was purchased from Becton Dickinson (BD), USA. The interleukin 4 (IL-4), lipopolysaccharide (LPS), interferon-$\gamma$ (IFN-$\gamma$), FITC-anti-CD86, and PE-anti-CD206 were obtained from Biolead, USA. All the commercially reagents were used as received unless otherwise noted.

**Instruments.** Fluorescence emission spectra were recorded on a RF-5301PC spectrofluorophotometer (Shimadzu, Japan) at room temperature. The upconversion luminescence spectra of UCNs and their nanoconjugates were measured at an angle of 90° to the excitation laser (808 nm) and an optical SEC-2000 spectrometer coupled 2048 pixels CCD assay (ALS Co., Ltd., Japan). A filter with short pass 750 nm was placed before the spectrometer to minimize scattering from the excitation laser beam. Transmission electron microscope (TEM) images were obtained using a FEI EM208S TEM (Philips) operated at 100 kV. Dynamic light scattering (DLS) and zeta potential measurements were performed by Brookhaven 90 Plus Nanoparticle Size Analyzer. The cell viabilities were measured by a Bio-Tek EL-311 microplate reader. Confocal imaging of living cells were carried out on Carl Zeiss LSM 800 confocal laser microscope (Germany). The upconversion imaging of cells were recorded on a Nikon confocal fluorescence microscope (Nikon, Eclipes TE2000-E, Japan) equipped with 980 nm NIR laser wide-field fluorescence add-on (EINST


DOI: 10.1021/acs.bioconjchem.8b00068
Bioconjugate Chem. 2018, 29, 928–938

Technology Pte Ltd., Singapore) in our lab. Flow cytometry (FCM) analysis was performed using a BD LSRFortessa X-20 cell analyzer (USA). Photoirradiation experiments were performed with an 808 nm NIR diode laser (Changchun New Industries Optoelectronics Technology Co., Ltd., China).

**Preparation of PUN Nanostructures.** *Synthesis of $NaYF_4$:Yb/Er/Nd (20/0.5/1%) Core UCNs.* Typically, the core UCNs were prepared by following the references published before.[23] 2 mL methanol containing $RE(CH_3CO_2)_3$ (RE = Y, Yb, Er, and Nd), 3 mL oleic acid, and 7 mL 1-octadecene were added in a 50 mL three-neck flask. The total lanthanide amount was 0.4 mmol and the ratio of Yb/Er/Nd was 20/0.5/1%. The mixture was heated to 150 °C for 60 min before cooling down to room temperature. Subsequently, a methanol solution (6 mL) containing $NH_4F$ (59.3 mg) and NaOH (40.0 mg) was added dropwisely and stirred for 30 min at 50 °C. Then methanol was evaporated and the solution was kept at 290 °C for 1.5 h under nitrogen atmosphere. After cooling down to room temperature, the core UCNs particles were precipitated by ethanol, washed several times by centrifugation, and redispersed in 4 mL hexane for the next step.

*Synthesis of $NaYF_4$:Yb/Tm/Nd (30/0.5/1%)@$NaYF_4$:Nd (20%) Core–Shell UCNs.* Typically, 3 mL oleic acid and 7 mL 1-octadecene were added in a 50 mL three-neck flask, then 2 mL methanol containing 0.4 mmol $RE(CH_3CO_2)_3$ (RE = Y/Nd (80/20%)) was also added in the solution. The mixture was heated to 150 °C for 60 min before cooling down to room temperature. Then the as-synthesized $NaYF_4$:Yb/Er/Nd core particles in 4 mL hexane were added along with a methanol solution (6 mL) containing $NH_4F$ (59.3 mg) and NaOH (40.0 mg). The resulting mixture was stirred for 30 min at 50 °C. After evaporating the methanol, the residual solution was kept at 290 °C for 1.5 h under nitrogen atmosphere and cooled down to room temperature. The UCNs were precipitated with ethanol and collected through centrifugation several times after ethanol washing. Finally, the core–shell UCNs were redispersed in 4 mL cyclohexane and conserved in the fridge at 4 °C.

*Synthesis of UCNs-PAA.* The as-prepared oleic acid capped UCNs (UCNs-OA) were precipitated using ethanol and redispersed in a 10 mL acid aqueous solution (pH = 4) adjusted by HCl (0.1 M). Then the solution was sonicated for 30 min followed by vigorous stirring for 2 h. During this reaction, the carboxylate groups of the oleate ligands were protonated (to yield oleic acid). Then the aqueous solution was extracted with 30 mL diethyl ether to remove the oleic acid three times. The combined ether layers were re-extracted with 10 mL water. Finally, the dispersible ligand-free UCNs in the water were recuperated by centrifugation (20000 rpm, 10 min) after precipitation with 20 mL acetone. The bare UCNs were redispersed in 20 mL water containing 200 mg of PAA (Mw = 1800) by sonication. The pH value was adjusted to 7.4 by NaOH (1 M) solution and stirred for 24 h at room temperature. After the reaction, the products (UCNs-PAA) were collected by centrifugation (20000 rpm for 10 min), washed with water for several times, and redispersed in water.

*Synthesis of UCNs-$MnO_2$.* Typically, 1 mL stock solution of UCNs-PAA (10 mg/mL) was added into a microcentrifuge tube containing 2.5 mL MES buffer (0.1 M, pH 6.0) followed by 2.5 mL $KMnO_4$ (100 mM) addition sequentially. The resulting mixture was sonicated for 30 min until a brown colloid solution was formed. The prepared UCNs-$MnO_2$ was collected by centrifugation (20000 rpm, 10 min), washed three times with water to remove the excess reactants, and redispersed in 1 mL water.

*Synthesis of UCNs-$MnO_2$-PEI.* The $MnO_2$-capped UCNs were encapsulated with branched PEI as reported previously.[23] Briefly, 10 mg of UCNs-$MnO_2$ in 1 mL water were activated by EDC·HCl (50 mg) and NHS (10 mg) for 30 min. Then the mixture was added dropwise to 2 mL PEI (10 mg/mL) in PBS (pH 7.4) followed by 30 min sonication. After 24 h magnetic stirring, the UCNs-$MnO_2$-PEI was purified by centrifugation (18000 rpm for 10 min) and washed three times with ethanol/water (1:1 v/v) to remove excess reactants.

*Synthesis of PUN (UCNs-$MnO_2$-Ce6-HA).* Generally, the Ce6 (1 mg) was first activated with EDC (23.0 mg) and NHS (13.8 mg) to form the active succinimidyl ester for 30 min, and added to the as-prepared UCNs-$MnO_2$-PEI solution for amide condensation reaction. After overnight magnetic stirring, the UCNs-$MnO_2$-Ce6 was purified by centrifugation (18000 rpm for 10 min) with ethanol/water (1:1 v/v) washing three times. Then HA (17.2 mg, 40 kDa) was also covalently anchored on the surface of prepared UCNs-$MnO_2$-Ce6 followed by the same reaction. The unreacted HA was removed by centrifugation (18000 rpm for 10 min) and washed three times with water. The final product (UCNs-$MnO_2$-Ce6-HA) was redispersed in 1 mL PBS (pH = 7.4) and stored in the fridge before use.

**Evaluation of Singlet Oxygen Generation of PUN in Buffers.** The singlet oxygen ($^1O_2$) generation was determined by a highly specific $^1O_2$ probe (SOSG) according to the protocol reported previously.[50] Briefly, SOSG (100 $\mu$g) was dissolved in 33 $\mu$L methanol as stock solution (5 mM). Different UCNs-based nanostructures including PUN containing Ce6 (1 $\mu$M) were mixed with SOSG (2.5 $\mu$M) in nitrogen-purged PBS (10 mM) with neutral (pH = 7.4) and acid conditions (pH = 5.5). After addition of $H_2O_2$ (10 mM) in different groups, and the solutions were stored in hypoxic and dark environment in a BD GasPak pouch anaerobic system, which could reduce oxygen tension to less than 2% within 2 h in a transparent plastic bag. Then the solutions in the hypoxic condition were irradiated with 808 nm NIR light laser (0.4 W/cm$^2$) for 1 h in the dark. The generated $^1O_2$ in different groups was recorded based on the enhanced fluorescence of SOSG at 530 nm compared with background signals ($E_x$: 494 nm).

**Cellular Uptake and Cytotoxicity Assessment of PUN in Living Tumor Cells.** The murine melanoma cell line (B16F10) was purchased from American Type Culture Collection (ATCC). The cells were cultured in DMEM supplemented with 10% FBS, 100 units/mL penicillin and 100 $\mu$g/mL streptomycin and maintained in a humidified incubator with 5% $CO_2$ at 37 °C. For cellular uptake study, the B16F10 cells were seeded in an ibidi confocal dish (35 mm, plastic bottom) at a density of $1 \times 10^5$ cells/well in 1 mL DMEM medium overnight. The dish was placed in a GasPak pouch anaerobic system for 24 h to generate the endogenous $H_2O_2$ by mimicking the hypoxic tumor microenvironment. Then the cells were incubated with PUN (100 $\mu$g/mL) for 8 h, washed two times with fresh DMEM, and stained with Hoechst 33342 by following the standard protocols for confocal imaging. For cell viability test, fresh log-phase B16F10 cells were seeded in a 96-well plate ($1 \times 10^4$ cells/well in 100 $\mu$L DMEM) and cultured for 24 h. The cells were incubated with different concentrations of PUNs for 8 h, washed with DMEM to remove free nanoparticles, and placed in a GasPak pouch anaerobic system for 4 h to mimic the hypoxic tumor microenvironment. Then the cells were exposed to 808 nm


DOI: 10.1021/acs.bioconjchem.8b00068
Bioconjugate Chem. 2018, 29, 928–938

NIR light irradiation at the power density of 0.4 W/cm$^2$ for 60 min in the dark (10 min break after 10 min irradiation). After 24 h incubation, the cell viabilities were determined by *in vitro* toxicology assay kit (TOX8, resazurin based) according to standard manufacturer's protocol.[52] For intracellular ROS level determination by FCM analysis and confocal imaging, the hypoxic cells were incubated with DCFDA (10 $\mu$M) in the dark for 30 min after treatment with various UCNs nanostructures (100 $\mu$g/mL) upon 808 nm NIR light irradiation (0.4 W/cm$^2$, 1 h). Each experiment was repeated three times and the average values were used for analysis.

**Immunomodulation of Tumor-Associated Macrophage (TAMs) Phenotype by PUN.** Typically, the murine monocyte macrophage RAW 264.7 cell line (M0-type) was purchased from American Type Culture Collection (ATCC). The cells were cultured in DMEM supplemented with 10% FBS, 100 units/mL penicillin, and 100 $\mu$g/mL streptomycin and maintained in a humidified incubator with 5% $CO_2$ at 37 °C. For macrophage polarization, the RAW264.7 cells were seeded in 6-well plate ($5 \times 10^5$ cells/well in 1 mL DMEM) and cultured overnight. The models of classically (M1-type) and alternatively (M2-type) activated macrophages were established by stimulating M0-type RAW 264.7 cells with IL-4 (50 ng/mL) and LPS (1 $\mu$g/mL)/IFN-$\gamma$ (50 ng/mL) for 24 h, respectively. The macrophage cells with different phenotypes were collected and seeded in an ibidi $\mu$-slide 4 well confocal dish ($5 \times 10^4$ cells/well in 0.5 mL DMEM) for overnight incubation. After fixing with methanol for 5 min and blocking by 1% BSA in PBS for 30 min at room temperature, the cells were stained with FITC-anti-CD86 (1 $\mu$g/mL) and PE-anti-CD206 (1 $\mu$g/mL) for 1 h. The free antibodies were removed by washing several times and the cells were observed by confocal imaging. For immunomodulation of M2-type TAMs with PUN, the macrophage cells were incubated with HA biopolymer (1 $\mu$M) at different molecular weight and PUN or other UCNs-based nanostructures (50 $\mu$g/mL) for 24 h. The reprogramed macrophage cells with different phenotypes were harvested by scraping and adjusted the cell suspension of $5 \times 10^5$ cells in ice cold PBS (200 $\mu$L) containing 10% FBS. Then FITC-anti-CD86 (1 $\mu$g) or PE-anti-CD206 (1 $\mu$g) was added into the cell suspension and incubated at room temperature for 45 min. Finally, the cells were washed three times with PBS by centrifugation (2000 rpm, 5 min) and resuspend in 1 mL PBS for FCM analysis.

**Inhibition of Tumor Cells Recurrence by PUN During post-PDT Period.** Normally, the RAW264.7 macrophage cells at different polarization states upon IL-4, LPS/IFN-$\gamma$, HA (40 kDa), PUN, and other UCNs-based nanostructures stimulation were prepared as previously, and seeded into a permeable transwell insert ($1 \times 10^5$ cells/well in DMEM). The B16F10 cells were seeded in 12-well plate ($5 \times 10^5$ cells/well in 1 mL DMEM) and incubated with PUN (200 $\mu$g/mL) as previously for PDT treatment in GasPak pouch anaerobic system upon 808 nm NIR light irradiation (0.4 W/cm$^2$, 1 h). After 24 h incubation in normoxia conditions, the medium was changed and the residual tumor cells were cocultured with the macrophages in the upper chamber of transwell insert upon different polarization states (M1 or M2 type). The tumor cells viabilities were determined every day after PDT treatment by a sensitive *in vitro* toxicology assay kit (TOX8) according to standard manufacturer's protocol.[52] The medium in the plate was collected at day 4 for detection of various cytokines based on mouse IL-6, IL-10, and TNF-$\alpha$ ELISA (enzyme-linked immunosorbent assay) kit according to the procedure described by the manufacturer (Beyotime Institute of Biotechnology, China). The standard solutions of these cytokines were incubated with tumor cells after PDT treatment to prove their cytoprotective or cytotoxic properties.

Moreover, the possible mechanism of tumor cell death upon M2-type TAM treatment was determined by FCM analysis using a standard Annexin V-FITC apoptosis assay kit.[59] Briefly, the M2-type RAW264.7 cells were incubated with HA (1 $\mu$M, 40 kDa), UCNs-$MnO_2$-Ce6 (50 $\mu$g/mL) and UCNs-$MnO_2$-Ce6-HA (PUN, 50 $\mu$g/mL) in the transwell supports for 24 h, respectively. The B16F10 cells were seeded in 12-well plates ($5 \times 10^5$ cells/well in 1 mL DMEM) and incubated with PUN (200 $\mu$g/mL) for PDT treatment upon 808 nm light irradiation as previously. After 24 h incubation, the residual tumor cells were cocultured with the macrophages at different polarization states in the upper chamber of transwell insert in the incubator for 3 days. The tumor cells were harvested with trypsin and resuspended in 1 × annexin-binding buffer to afford the dilute cells density ($5 \times 10^5$ cells in 200 $\mu$L binding buffer). Then 5 $\mu$L Annexin V-FITC solutions (100 $\mu$g/mL) were added to the cell suspension for 15 min incubation at room temperature. After washing with binding buffer for two times, the cells were resuspended in 200 $\mu$L binding buffer and stained with 5 $\mu$L propidium iodide (PI) solutions (100 $\mu$g/mL) for another 15 min incubation at room temperature. The free regents were removed by washing two times and the cells samples were mixed gently within 400 $\mu$L ice-cold binding buffer for FCM analysis. The cells were enumerated by BD LSRFortessa X-20 flow cytometer (FITC: $E_x$: 488 nm, $E_m$: 525/50 nm; PI: $E_x$: 532 nm, $E_m$: 610/20 nm). Usually, in each panel of FCM analysis, the lower left quadrant shows the healthy cells (Annexin V-FITC$^-$/PI$^-$), the lower right quadrant shows early stage apoptotic cells (Annexin V-FITC$^+$/PI$^-$), the upper right quadrant shows late-stage apoptotic cells (Annexin V-FITC$^+$/PI$^+$), and the upper left quadrant shows necrotic cells (Annexin V-FITC$^-$/PI$^+$), respectively. The percentage of necrotic, early, and late apoptotic cells indicates the cell damage upon M2-type TAMs treatment. The results were processed with FlowJo 7.6.1 software.

## ■ ASSOCIATED CONTENT

### Supporting Information

The Supporting Information is available free of charge on the ACS Publications website at DOI: 10.1021/acs.bioconjchem.8b00068.

TEM images; UV−vis absorption spectra; FTIR spectroscopy; UCL spectra; DLS results; confocal imaging analysis; FCM analysis; scheme of the process for loading amount determination of HA on the PUN surface (PDF)

## ■ AUTHOR INFORMATION


### Corresponding Author

*E-mail: Bengang@ntu.edu.sg.

### ORCID

Juan Li: 0000-0001-7175-2320

Huanghao Yang: 0000-0001-5894-0909

Bengang Xing: 0000-0002-8391-1234


### Notes

The authors declare no competing financial interest.



DOI: 10.1021/acs.bioconjchem.8b00068
*Bioconjugate Chem.* 2018, 29, 928−938

## ■ ACKNOWLEDGMENTS

The authors acknowledge the financial supports by NTU-AIT-MUV NAM/16001, RG110/16 (S), (RG 11/13) and (RG 35/15) awarded in Nanyang Technological University, Singapore and National Natural Science Foundation of China (NSFC) (No. 51628201).

## ■ REFERENCES

(1) Aggarwal, S. (2010) Targeted cancer therapies. *Nat. Rev. Drug Discovery 9*, 427−428.
(2) Gotwals, P., Cameron, S., Cipolletta, D., Cremasco, V., Crystal, A., Hewes, B., Mueller, B., Quaratino, S., Sabatos-Peyton, C., and Petruzzelli, L. (2017) Prospects for combining targeted and conventional cancer therapy with immunotherapy. *Nat. Rev. Cancer 17*, 286−301.
(3) Khalil, D. N., Smith, E. L., Brentjens, R. J., and Wolchok, J. D. (2016) The future of cancer treatment: immunomodulation, CARs and combination immunotherapy. *Nat. Rev. Clin. Oncol. 13*, 273−290.
(4) Cai, Y., Shen, H., Zhan, J., Lin, M., Dai, L., Ren, C., Shi, Y., Liu, J., Gao, J., and Yang, Z. (2017) Supramolecular "Trojan Horse" for Nuclear Delivery of Dual Anticancer Drugs. *J. Am. Chem. Soc. 139*, 2876−2879.
(5) Yang, Y., Velmurugan, B., Liu, X., and Xing, B. (2013) NIR photoresponsive crosslinked upconverting nanocarriers toward selective intracellular drug release. *Small 9*, 2937−2944.
(6) Castano, A. P., Mroz, P., and Hamblin, M. R. (2006) Photodynamic therapy and anti-tumour immunity. *Nat. Rev. Cancer 6*, 535−545.
(7) Lucky, S. S., Soo, K. C., and Zhang, Y. (2015) Nanoparticles in photodynamic therapy. *Chem. Rev. 115*, 1990−2042.
(8) Hu, J., Tang, Y. a., Elmenoufy, A. H., Xu, H., Cheng, Z., and Yang, X. (2015) Nanocomposite-Based Photodynamic Therapy Strategies for Deep Tumor Treatment. *Small 11*, 5860−5887.
(9) Kobayashi, H., Ogawa, M., Alford, R., Choyke, P. L., and Urano, Y. (2010) New strategies for fluorescent probe design in medical diagnostic imaging. *Chem. Rev. 110*, 2620−2640.
(10) Ai, X., Mu, J., and Xing, B. (2016) Recent Advances of Light-Mediated Theranostics. *Theranostics 6*, 2439−2457.
(11) Shanmugam, V., Selvakumar, S., and Yeh, C.-S. (2014) Near-infrared light-responsive nanomaterials in cancer therapeutics. *Chem. Soc. Rev. 43*, 6254−6287.
(12) Zhang, Z., Wang, J., and Chen, C. (2013) Near-Infrared Light-Mediated Nanoplatforms for Cancer Thermo-Chemotherapy and Optical Imaging. *Adv. Mater. 25*, 3869−3880.
(13) Huang, L., Li, Z., Zhao, Y., Zhang, Y., Wu, S., Zhao, J., and Han, G. (2016) Ultralow-power near infrared lamp light operable targeted organic nanoparticle photodynamic therapy. *J. Am. Chem. Soc. 138*, 14586−14591.
(14) Huang, L., Li, Z., Zhao, Y., Yang, J., Yang, Y., Pendharkar, A. I., Zhang, Y., Kelmar, S., Chen, L., Wu, W., Zhao, J., and Han, G. (2017) Enhancing Photodynamic Therapy through Resonance Energy Transfer Constructed Near-Infrared Photosensitized Nanoparticles. *Adv. Mater. 29*, 1604789−1604795.
(15) Anderson, E. D., Gorka, A. P., and Schnermann, M. J. (2016) Near-infrared uncaging or photosensitizing dictated by oxygen tension. *Nat. Commun. 7*, 13378.
(16) Barth, B. M., Altinoğlu, E. I., Shanmugavelandy, S. S., Kaiser, J. M., Crespo-Gonzalez, D., DiVittore, N. A., McGovern, C., Goff, T. M., Keasey, N. R., and Adair, J. H. (2011) Targeted indocyanine-green-loaded calcium phosphosilicate nanoparticles for in vivo photodynamic therapy of leukemia. *ACS Nano 5*, 5325−5337.
(17) Fan, W., Bu, W., and Shi, J. (2016) On The Latest Three-Stage Development of Nanomedicines based on Upconversion Nanoparticles. *Adv. Mater. 28*, 3987−4011.
(18) Wu, X., Zhang, Y., Takle, K., Bilsel, O., Li, Z., Lee, H., Zhang, Z., Li, D., Fan, W., Duan, C., Chan, E. M., Lois, C., Xiang, Y., and Han, G. (2016) Dye-sensitized core/active shell upconversion nanoparticles for optogenetics and bioimaging applications. *ACS Nano 10*, 1060−1066.
(19) Yang, Y., Shao, Q., Deng, R., Wang, C., Teng, X., Cheng, K., Cheng, Z., Huang, L., Liu, Z., Liu, X., and Xing, B. (2012) In vitro and in vivo uncaging and bioluminescence imaging by using photocaged upconversion nanoparticles. *Angew. Chem., Int. Ed. 51*, 3125−3129.
(20) Yao, C., Wang, W., Wang, P., Zhao, M., Li, X., and Zhang, F. (2018) Near-Infrared Upconversion Mesoporous Cerium Oxide Hollow Biophotocatalyst for Concurrent pH-/H2O2-Responsive O2-Evolving Synergetic Cancer Therapy. *Adv. Mater. 30*, 1704833.
(21) Dong, H., Sun, L. D., Li, L. D., Si, R., Liu, R., and Yan, C. H. (2017) Selective Cation Exchange Enabled Growth of Lanthanide Core/Shell Nanoparticles with Dissimilar Structure. *J. Am. Chem. Soc. 139*, 18492−18495.
(22) Idris, N. M., Gnanasammandhan, M. K., Zhang, J., Ho, P. C., Mahendran, R., and Zhang, Y. (2012) In vivo photodynamic therapy using upconversion nanoparticles as remote-controlled nanotransducers. *Nat. Med. 18*, 1580−1585.
(23) Ai, X., Ho, C. J. H., Aw, J., Attia, A. B. E., Mu, J., Wang, Y., Wang, X., Wang, Y., Liu, X., Chen, H., Gao, M., Chen, X., Yeow, E. K. L., Liu, G., Olivo, M., and Xing, B. (2016) In vivo covalent cross-linking of photon-converted rare-earth nanostructures for tumour localization and theranostics. *Nat. Commun. 7*, 10432.
(24) Yang, D., Hou, Z., Cheng, Z., Li, C., and Lin, J. (2015) Current advances in lanthanide ion ($Ln^{3+}$)-based upconversion nanomaterials for drug delivery. *Chem. Soc. Rev. 44*, 1416−1448.
(25) Huang, L., Zhao, Y., Zhang, H., Huang, K., Yang, J., and Han, G. (2017) Expanding Anti-Stokes Shifting in Triplet-Triplet Annihilation Upconversion for In Vivo Anticancer Prodrug Activation. *Angew. Chem., Int. Ed. 56*, 14400−14404.
(26) Ai, X., Lyu, L., Mu, J., Hu, M., Wang, Z., and Xing, B. (2017) Synthesis of Core-shell Lanthanide-doped Upconversion Nanocrystals for Cellular Applications. *J. Visualized Exp. 129*, No. e56416, DOI: 10.3791/56416.
(27) Cheng, Y., Cheng, H., Jiang, C., Qiu, X., Wang, K., Huan, W., Yuan, A., Wu, J., and Hu, Y. (2015) Perfluorocarbon nanoparticles enhance reactive oxygen levels and tumour growth inhibition in photodynamic therapy. *Nat. Commun. 6*, 8785.
(28) Liu, Y., Liu, Y., Bu, W., Cheng, C., Zuo, C., Xiao, Q., Sun, Y., Ni, D., Zhang, C., Liu, J., and Shi, J. (2015) Hypoxia Induced by Upconversion-Based Photodynamic Therapy: Towards Highly Effective Synergistic Bioreductive Therapy in Tumors. *Angew. Chem., Int. Ed. 54*, 8105−8109.
(29) Zhou, N., Cao, X., Du, X., Wang, H., Wang, M., Liu, S., Nguyen, K., Schmidt Rohr, K., Xu, Q., and Liang, G. (2017) Hyper-Crosslinkers Lead to Temperature-and pH-Responsive Polymeric Nanogels with Unusual Volume Change. *Angew. Chem., Int. Ed. 56*, 2623−2627.
(30) Hai, Z., Li, J., Wu, J., Xu, J., and Liang, G. (2017) Alkaline Phosphatase-Triggered Simultaneous Hydrogelation and Chemiluminescence. *J. Am. Chem. Soc. 139*, 1041−1044.
(31) Jordan, B. F., and Sonveaux, P. (2012) Targeting tumor perfusion and oxygenation to improve the outcome of anticancer therapy. *Front. Pharmacol. 3*, 94.
(32) Cook, C. C., Kim, A., Terao, S., Gotoh, A., and Higuchi, M. (2012) Consumption of oxygen: a mitochondrial-generated progression signal of advanced cancer. *Cell Death Dis. 3*, e258.
(33) Rockwell, S., Dobrucki, I. T., Kim, E. Y., Marrison, S. T., and Vu, V. T. (2009) Hypoxia and radiation therapy: past history, ongoing research, and future promise. *Curr. Mol. Med. 9*, 442−458.
(34) Quail, D. F., and Joyce, J. A. (2013) Microenvironmental regulation of tumor progression and metastasis. *Nat. Med. 19*, 1423−1437.
(35) Georgoudaki, A.-M., Prokopec, K. E., Boura, V. F., Hellqvist, E., Sohn, S., Östling, J., Dahan, R., Harris, R. A., Rantalainen, M., and Klevebring, D. (2016) Reprogramming tumor-associated macrophages by antibody targeting inhibits cancer progression and metastasis. *Cell Rep. 15*, 2000−2011.
(36) De Palma, M., and Lewis, C. E. (2013) Macrophage regulation of tumor responses to anticancer therapies. *Cancer Cell 23*, 277−286.


DOI: 10.1021/acs.bioconjchem.8b00068
*Bioconjugate Chem.* 2018, 29, 928−938

(37) Murray, P. J., and Wynn, T. A. (2011) Protective and pathogenic functions of macrophage subsets. *Nat. Rev. Immunol. 11*, 723−737.
(38) Noy, R., and Pollard, J. W. (2014) Tumor-associated macrophages: from mechanisms to therapy. *Immunity 41*, 49−61.
(39) Martinez, F. O., and Gordon, S. (2014) The M1 and M2 paradigm of macrophage activation: time for reassessment. *F1000Prime Rep. 6*, 13.
(40) Tatano, Y., Shimizu, T., and Tomioka, H. (2015) Unique macrophages different from M1/M2 macrophages inhibit T cell mitogenesis while upregulating Th17 polarization. *Sci. Rep. 4*, 4146.
(41) Fan, W., Bu, W., Shen, B., He, Q., Cui, Z., Liu, Y., Zheng, X., Zhao, K., and Shi, J. (2015) Intelligent MnO2 Nanosheets Anchored with Upconversion Nanoprobes for Concurrent pH-/H2O2-Responsive UCL Imaging and Oxygen-Elevated Synergetic Therapy. *Adv. Mater. 27*, 4155−4161.
(42) Yang, G., Xu, L., Chao, Y., Xu, J., Sun, X., Wu, Y., Peng, R., and Liu, Z. (2017) Hollow MnO 2 as a tumor-microenvironment-responsive biodegradable nano-platform for combination therapy favoring anti-tumor immune responses. *Nat. Commun. 8*, 902.
(43) Song, M., Liu, T., Shi, C., Zhang, X., and Chen, X. (2016) Bioconjugated manganese dioxide nanoparticles enhance chemotherapy response by priming tumor-associated macrophages toward M1-like phenotype and attenuating tumor hypoxia. *ACS Nano 10*, 633−647.
(44) Rayahin, J. E., Buhrman, J. S., Zhang, Y., Koh, T. J., and Gemeinhart, R. A. (2015) High and low molecular weight hyaluronic acid differentially influence macrophage activation. *ACS Biomater. Sci. Eng. 1*, 481−493.
(45) Tran, T. H., Rastogi, R., Shelke, J., and Amiji, M. M. (2015) Modulation of macrophage functional polarity towards anti-inflammatory phenotype with plasmid DNA delivery in CD44 targeting hyaluronic acid nanoparticles. *Sci. Rep. 5*, 16632.
(46) Deng, R., Xie, X., Vendrell, M., Chang, Y.-T., and Liu, X. (2011) Intracellular glutathione detection using MnO2-nanosheet-modified upconversion nanoparticles. *J. Am. Chem. Soc. 133*, 20168−20171.
(47) Muhr, V., Wilhelm, S., Hirsch, T., and Wolfbeis, O. S. (2014) Upconversion nanoparticles: from hydrophobic to hydrophilic surfaces. *Acc. Chem. Res. 47*, 3481−3493.
(48) Wu, X., Chen, G., Shen, J., Li, Z., Zhang, Y., and Han, G. (2015) Upconversion nanoparticles: a versatile solution to multiscale biological imaging. *Bioconjugate Chem. 26*, 166−175.
(49) Prasad, P., Gordijo, C. R., Abbasi, A. Z., Maeda, A., Ip, A., Rauth, A. M., DaCosta, R. S., and Wu, X. Y. (2014) Multifunctional albumin-$MnO_2$ nanoparticles modulate solid tumor microenvironment by attenuating hypoxia, acidosis, vascular endothelial growth factor and enhance radiation response. *ACS Nano 8*, 3202−3212.
(50) Huang, P., Lin, J., Wang, X., Wang, Z., Zhang, C., He, M., Wang, K., Chen, F., Li, Z., and Shen, G. (2012) Light-triggered theranostics based on photosensitizer-conjugated carbon dots for simultaneous enhanced-fluorescence imaging and photodynamic therapy. *Adv. Mater. 24*, 5104−5110.
(51) Koshikawa, N., Iyozumi, A., Gassmann, M., and Takenaga, K. (2003) Constitutive upregulation of hypoxia-inducible factor-1$\alpha$ mRNA occurring in highly metastatic lung carcinoma cells leads to vascular endothelial growth factor overexpression upon hypoxic exposure. *Oncogene 22*, 6717−6724.
(52) Ai, X., Lyu, L., Zhang, Y., Tang, Y., Mu, J., Liu, F., Zhou, Y., Zuo, Z., Liu, G., and Xing, B. (2017) Remote Regulation of Membrane Channel Activity by Site-Specific Localization of Lanthanide-Doped Upconversion Nanocrystals. *Angew. Chem., Int. Ed. 56*, 3031−3035.
(53) Wu, D., and Yotnda, P. (2011) Production and detection of reactive oxygen species (ROS) in cancers. *J. Visualized Exp. 57*, 3357.
(54) Patel, S. K., and Janjic, J. M. (2015) Macrophage targeted theranostics as personalized nanomedicine strategies for inflammatory diseases. *Theranostics 5*, 150−172.
(55) Lu, G., Zhang, R., Geng, S., Peng, L., Jayaraman, P., Chen, C., Xu, F., Yang, J., Li, Q., and Zheng, H. (2015) Myeloid cell-derived inducible nitric oxide synthase suppresses M1 macrophage polarization. *Nat. Commun. 6*, 6676.
(56) Luo, Z., Wu, Q., Yang, C., Wang, H., He, T., Wang, Y., Wang, Z., Chen, H., Li, X., Gong, C., and Yang, Z. (2017) A Powerful CD8+ T-Cell Stimulating D-Tetra-Peptide Hydrogel as a Very Promising Vaccine Adjuvant. *Adv. Mater. 29*, 1601776.
(57) He, H., Zhang, S., Tighe, S., Son, J., and Tseng, S. C. (2013) Immobilized heavy chain-hyaluronic acid polarizes lipopolysaccharide-activated macrophages toward M2 phenotype. *J. Biol. Chem. 288*, 25792−25803.
(58) Scheibner, K. A., Lutz, M. A., Boodoo, S., Fenton, M. J., Powell, J. D., and Horton, M. R. (2006) Hyaluronan fragments act as an endogenous danger signal by engaging TLR2. *J. Immunol. 177*, 1272−1281.
(59) Thomas, E., Gopalakrishnan, V., Somasagara, R. R., Choudhary, B., and Raghavan, S. C. (2016) Extract of vernonia condensata, inhibits tumor progression and improves survival of tumor-allograft bearing mouse. *Sci. Rep. 6*, 23255.


DOI: 10.1021/acs.bioconjchem.8b00068
*Bioconjugate Chem.* 2018, 29, 928−938